CHINESE OPTICS LETTERS

Vol. 22, No. 4 | April 2024

1.6-μm single-frequency erbium-doped fiber laser based on two cascaded subrings

Yaqi Zhai (翟雅琦)[1,2], Han Wen (文 瀚)[1,2], Haowei Chen (陈浩伟)[1,2*], Baole Lu (陆宝乐)[1,2**], and Jintao Bai (白晋涛)[1,2]

[1] State Key Laboratory of Energy Photon-Technology in Western China, International Collaborative Center on Photoelectric Technology and Nano Functional Materials, Institute of Photonics & Photon-Technology, Northwest University, Xi'an 710127, China

[2] Shaanxi Engineering Technology Research Center for Solid State Lasers and Application, Shaanxi Provincial Key Laboratory of Photo-electronic Technology, Northwest University, Xi'an 710127, China

*Corresponding author: chenhaowei0320@163.com

**Corresponding author: lubaole1123@163.com

Received November 20, 2023 | Accepted January 2, 2024 | Posted Online April 26, 2024

We demonstrate a stable narrow linewidth single-frequency erbium-doped fiber laser (EDFL) operating at 1.6 μm. A Fabry–Perot fiber Bragg grating and two cascaded subrings are incorporated in the main ring cavity to achieve single-frequency operation. The experimentally measured optical signal-to-noise ratio is greater than 73 dB. Furthermore, the linewidth of the EDFL is measured to be about 480 Hz by the self-built short-delayed self-heterodyne interferometry device. The laser shows superior stability, with no mode-hopping during the 60-min observation period. The proposed EDFL provides a new experimental idea for realizing a single-frequency fiber laser in the L-band.

Keywords: erbium-doped fiber laser; two cascaded subrings; single frequency.
DOI: 10.3788/COL202422.041406

1. Introduction

Single-frequency fiber lasers (SFFLs) with narrow linewidth, excellent coherence, and high optical signal-to-noise ratio (OSNR) have been widely used in the fields of optical fiber sensors, optical fiber communication, atmospheric remote sensing, lidar, and high-resolution spectroscopy[1–7]. With the increase in the demand for optical communications transmission capacity, there is an urgent need to expand the laser wavelength from the traditional C-band to the L-band covering 1.6 μm. In addition, the L-band is an eye-safe band and has a high penetration capacity for smoke, so the development of 1.6 μm lasers has potential applications promising for atmospheric remote sensing[8]. Fortunately, the absorption-emission spectrum of erbium-doped fiber (EDF) contains the L-band. Although the L-band is located at the emission edge of Er^{3+} with a small emission cross section, it has been found that this can be improved by increasing the pump power or the length of the gain fiber. Moreover, using longer EDF not only suppresses the amplified spontaneous emission (ASE) in the C-band but also provides sufficient gain to achieve the L-band lasers.

Compared with 1.6 μm all-solid lasers, all-fiber lasers have the advantages of high conversion efficiency, excellent beam quality, and low environmental impact[9]. Depending on the cavity type, the SFFLs can be divided into linear and ring cavities[10]. In general, linear cavities require active fibers to be short enough and narrower-band gratings to achieve single-frequency (SF) operation, as well as tight temperature control and vibration isolation devices to improve stability. Compared to linear cavity, fiber lasers based on a ring cavity avoid the standing wave-induced spatial hole-burning (SHB) effect. However, the EDF uniform broadening phenomenon and long fiber lead to strong longitudinal-modes competition and smaller mode spacing, which can be flexibly improved by adding high-precision filters in the cavity[11,12], such as by adding subrings structure[13], saturable absorbers[14], ultranarrow filters[15], and Mach–Zehnder interferometers[16]. In recent years, several articles have reported the realization of 1.6 μm SFFLs. Yang *et al.* achieved an output wavelength of 1603 nm using a distributed Bragg reflector laser formed by a 16-mm-long Er^{3+}/Yb^{3+} co-doped gain fiber and a highly reflective fiber Bragg grating (FBG)[17]. The laser can achieve a high output power, but its stability remains a challenge, limiting practical applications. Hang *et al.* implemented a ring cavity SFFL using a 5.2 m-long EDF as the gain medium in combination with a narrowband filter[18]. They achieved tunable laser output in the C + L band, but the OSNR in the 1.6 μm was low, less than 60 dB. Yang *et al.* achieved a ring cavity SFFL with an operating wavelength of 1608 nm using a 1480 nm laser diode (LD) pumping a homemade high-concentration erbium-doped silica fiber[19]. Their linewidth was obtained using the long-delay self-heterodyne interferometry technique, which introduces additional loss. Up to now, the

linewidth of 1.6 μm ring cavity SF erbium-doped fiber laser (EDFL) based on the short-delay self-heterodyne interferometry (SDSHI) method measurement has not been reported yet.

In this paper, we report an SF EDFL based on a Fabry–Perot fiber Bragg grating (FP-FBG) and two cascaded subrings (TCSRs). A narrow bandwidth FBG is used to determine the operating wavelength of the laser at 1600.06 nm, which is combined with an FP-FBG as well as the TCSRs device to achieve stable SF operation. The experimental results show that the OSNR of the output wavelength is higher than 73 dB. The linewidth is measured of 480 Hz by using a self-constructed SDSHI setup. The SDSHI only needs a few kilometers of fiber delay, reducing the influence of changes such as fiber introduction loss and noise introduction on the laser linewidth. In addition, we measure the longitudinal-mode stability of the laser and find no mode-hopping phenomenon, which indicates that the EDFL operates in a stable SF state. The proposed 1.6 μm SF EDFL with narrow linewidth and high OSNR shows potential applications in coherent lidar and long-distance coherent optical communications.

2. Experimental Setup and Principle

The experimental setup of the 1.6 μm SF EDFL is illustrated in Fig. 1. The 976 nm LD is coupled into the cavity through a 976/1600 nm wavelength division multiplexer (WDM). A 1.8 m commercial EDF (LIEKKI Er110-4/125) with a core absorption coefficient of 110 dB/m at 1530 nm is used as the gain medium. A circulator (CIR) acts as an isolator, ensuring unidirectional propagation of the light and preventing the effect of SHB. The FBG is connected to port 2 of the CIR and reflects light signals of specific wavelengths to port 3 of the CIR. The FP-FBG is connected to port 3 of the CIR. An FC/APC is fused at the transmission port of the FBG to reduce the effect of the reflected light from the fiber end face. A polarization controller (PC) is used to regulate the polarization state. To ensure single-longitudinal-mode (SLM) operation, two 50:50 optical couplers (OC1 and OC2) are added to form TCSRs as a high-precision filter. A 10:90 OC3 is used as the output element, with the 90% port connected to the main cavity to maintain operation and the 10% port used for extracting the laser to be measured. The length of the ring cavity is ~13.77 m, corresponding to a longitudinal-mode spacing of ~14.82 MHz. All devices used in this experiment are placed on an optical platform to avoid interference from external vibrations.

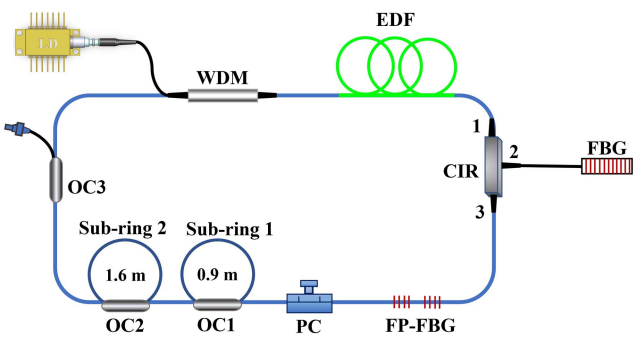

Fig. 1. Experimental setup of the 1.6 μm SF EDFL.

The reflection spectrum of FBG and the transmission spectrum of FP-FBG are detected by an ASE, as shown in Fig. 2, which is measured by an optical spectrum analyzer (OSA, Yokogawa, AQ6370C) with a resolution of 0.02 nm. The inset shows an enlarged view of the blue dashed section. The central wavelength of the FBG reflection peak is 1600.06 nm, with reflectivity greater than 95% and a 3 dB bandwidth of 0.15 nm, corresponding to 17.58 GHz. The 3 dB bandwidth of FP-FBG is 0.1 nm, which corresponds to 11.72 GHz. In the transmission spectrum simulation of FP-FBG, the transmission effect is better when the cavity length of FP-FBG and the grating length of the two sub-gratings are both 10 mm. If the cavity length is too long then the number of transmission peaks increases and the spacing between neighboring transmission peaks becomes small, which is easy to cause mode competition; if the sub-grating region length is too small, the 3 dB bandwidth becomes large and the transmission depth becomes shallow. It is worth noting that the parameters of the two sub-gratings are exactly the same. However, the presence of minor axial stress in the fiber makes the actual measured spectrum characteristics deviate slightly from the simulation. From Fig. 2, it can be seen that the FP-FBG has three transmission peaks. Still, only the transmission peaks (blue dashed line in the illustration) within the reflection peaks of the FBG can oscillate, so it does not affect the longitudinal-mode selectivity of the FP-FBG and still satisfies the filtering condition. The combination of FBG and FP-FBG acts as a wavelength selector and filter, which can reduce a large number of longitudinal modes but is not enough to achieve SF operation, so the laser is still in the state of multiple longitudinal modes at this time.

Considering the simplicity and effectiveness of realizing SF, the TCSRs are formed by using two 50:50 OCs (OC1, OC2) in the experiment. TCSRs can effectively increase the longitudinal-mode spacing and reduce the mode-hopping phenomenon. According to the Vernier effect[20], only longitudinal modes that meet the resonance conditions of each subring

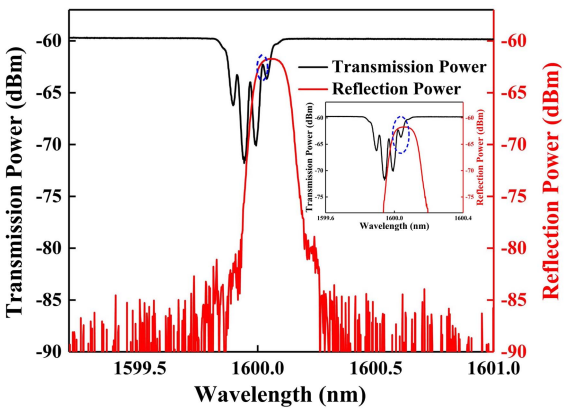

Fig. 2. Transmission spectrum of the FP-FBG and reflection spectrum of the FBG.

can be oscillated. In addition, in order to select the SLM from the main ring cavity (MRC) dense longitudinal modes, the 3 dB bandwidth of passband of the TCSRs should be 1–2 times the spacing of the neighboring longitudinal modes. The effective free spectrum range (FSR) of TCSRs should be no less than half of the 3 dB bandwidth of FP-FBG[21,22].

The transmission schematic of the TCSRs filter is shown in Fig. 3. The optical path of the TCSRs can be expressed as: 1(OC1)→4(OC1)→2(OC1)→3(OC1)→5(OC2)→8(OC2)→6(OC2)→7(OC2), where the numbers 1–8 represent the port number of each OC, and E_1–E_8 represent the electric field amplitude of each port. L_1–L_3 are the connection length of each OC. In Ring-1, the transmission relationship of E_3 and E_1 is expressed as[23,24]

$$\frac{E_3}{E_1}=\sqrt{1-\alpha_1}\,\frac{\sqrt{1-\gamma_1}-\sqrt{1-\alpha_1}\sqrt{1-\delta_1}e^{-\beta L_1}e^{i\omega\tau_1}}{1-\sqrt{1-\delta_1}\sqrt{1-\alpha_1}\sqrt{1-\gamma_1}e^{-\beta L_1}e^{i\omega\tau_1}}. \quad (1)$$

Similarly, in Ring-2, the field transmission relationship of E_7 and E_5 can be expressed as

$$\frac{E_7}{E_5}=\sqrt{1-\alpha_2}\,\frac{\sqrt{1-\gamma_2}-\sqrt{1-\alpha_2}\sqrt{1-\delta_2}e^{-\beta L_2}e^{i\omega\tau_2}}{1-\sqrt{1-\delta_2}\sqrt{1-\alpha_2}\sqrt{1-\gamma_2}e^{-\beta L_2}e^{i\omega\tau_2}}. \quad (2)$$

The transmission relationship between E_5 and E_3 is

$$E_5=\sqrt{1-\delta}e^{i\omega\tau_3}e^{-\beta L_3}E_3. \quad (3)$$

Therefore, the transmission T of the TCSRs filter can be obtained as

$$\begin{aligned}T&=\left(\frac{E_7}{E_1}\right)\cdot\left(\frac{E_7}{E_1}\right)^*\\&=\left(\sqrt{1-\delta}e^{-\beta L_3}e^{i\omega\tau_3}\frac{E_3}{E_1}\frac{E_7}{E_5}\right)\left(\sqrt{1-\delta}e^{-\beta L_3}e^{i\omega\tau_3}\frac{E_3}{E_1}\frac{E_7}{E_5}\right)^*. \quad (4)\end{aligned}$$

α is the insertion loss of the coupler, δ is the fusion splice loss of the fiber, γ is the optical coupling ratio of the coupler, β is the loss factor of the fiber, ω is the optical field angular frequency, and τ_i corresponds to the fiber delay. The 3 dB bandwidth of the passive ring cavity can be expressed as[12]

$$\Delta\nu'=\frac{c\psi}{2\pi nL},\qquad \psi=\ln\left(\frac{I_{\rm in}}{I_{\rm out}}\right), \quad (5)$$

where ψ is the unidirectional loss of the cavity, n is the refractive index of the fiber core and is 1.47, $c=3\times10^8$ m/s is the speed of light in vacuum, and $I_{\rm in}$ and $I_{\rm out}$ are the input and output laser intensities, respectively. Based on the above theory, the results of the transmission spectrum of the TCSRs filter can be simulated as shown in Fig. 4. Through continuous optimization, we finally calculated the length of Ring-1 to be 0.9 m with a corresponding FSR of 226 MHz and the length of Ring-2 to be 1.6 m with a corresponding FSR of 126 MHz, according to[25] FSR $=\frac{c}{nL_i}$. The effective FSR is 14.23 GHz, which corresponds to 0.12 nm. It is larger than the bandwidth of the FP-FBG transmission spectrum and smaller than the bandwidth of the FBG reflection peak. The purpose of the short ring is to enlarge the effective FSR, while the long ring benefits the narrow 3 dB bandwidth. According to Eq. (5), the passband bandwidth of the Ring-2 is calculated to be ~15.6 MHz. This guarantees that only one longitudinal mode can pass through the transmission band of the TCSRs filter. Therefore, the SLM operation can be achieved theoretically.

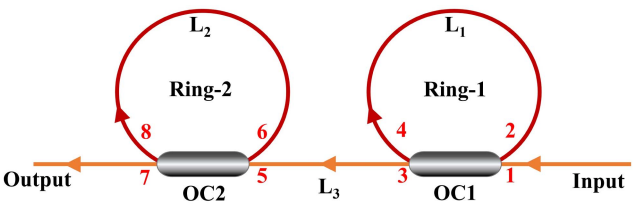

Fig. 3. Schematic of the TCSRs filter.

3. Experimental Results and Discussion

The experiment is operated at room temperature, and no other vibration isolation or temperature compensation techniques are performed. The oscillation threshold of EDFL is 275 mW. As shown in Fig. 5(a), the measured OSNR is ~75 dB when the pump power is 345 mW and the central wavelength is 1600.06 nm with a resolution of 0.02 nm. High OSNR reflects the superior oscillation quality of the laser and the excellent mode selection ability of the filter. Figure 5(b) demonstrates the output spectrum at different pump powers. From the inset of Fig. 5(b), it is found that the measured OSNR increases with the improvement of pump powers. Furthermore, the OSNR is greater than 73 dB for any pump power, which indicates that the proposed TCSRs configuration ensures a high Q-factor for EDFL.

The longitudinal-mode characteristics of the output signal are verified by the self-homodyne method at the same pump power. Figure 6 illustrates a plot of the beating signal measured using a photodetector (PD, Thorlabs, DET08CFC/M) and a radio-frequency (RF) electrical spectrum analyzer (ESA,

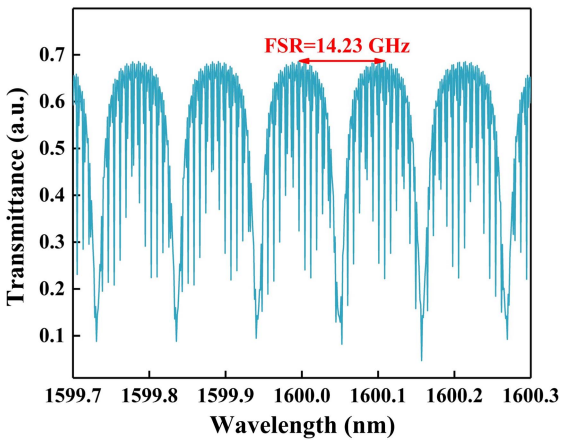

Fig. 4. Simulated transmission spectrum of TCSRs.

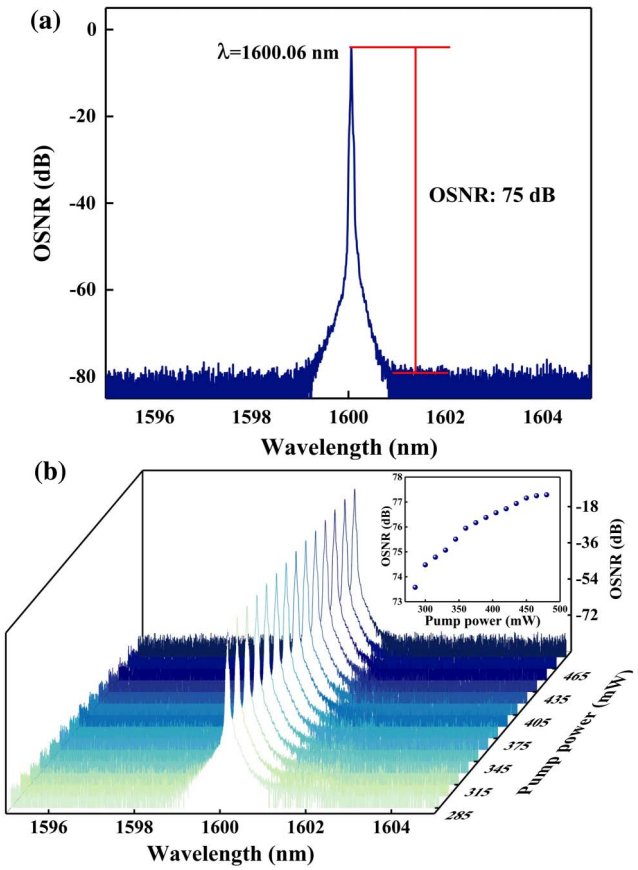

Fig. 5. (a) Output spectrum of the EDFL at the pump power of 345 mW; (b) output OSNR of the EDFL at different pump powers.

Keysight, N9000B). The ESA has a scanning range of 200 MHz, a resolution bandwidth (RBW) of 100 kHz, and a view resolution bandwidth of 1 kHz. Figure 6(a) demonstrates the RF beating signal when the filter in the ring cavity only has FBG. A large number of beating signals can be seen, and the spacing of the adjacent longitudinal modes is 14.82 MHz, which is a multilongitudinal-mode state. To further investigate the mode-selection ability of the TCSR filter, the TCSRs are replaced by a section of single-mode fiber to maintain the original MRC length, as shown in Fig. 6(b). It can be seen that the longitudinal modes are reduced and the longitudinal-mode spacing is unchanged when the filtering devices in the cavity have FBG and FP-FBG. At the same time, this also shows the filtering ability of FP-FBG. After that, the TCSRs filter is added in the MRC, and by carefully adjusting the PC, no beating signal is seen in the scan range, as shown in Fig. 6(c), proving that the EDFL is working in the SF state.

The output stability of the EDFL is measured as shown in Fig. 7. Figure 7(a) shows the variation of wavelength and output power in 60 min. The wavelength is stabilized at 1600.06 nm, the fluctuation of the wavelength is less than the limiting resolution of 0.02 nm for OSA, and the change of the output power is less than 0.169 dB. The tiny fluctuations of the wavelength and the power are mainly caused by the fluctuation of the RIN of the pump source and the vibration of the environment. To monitor

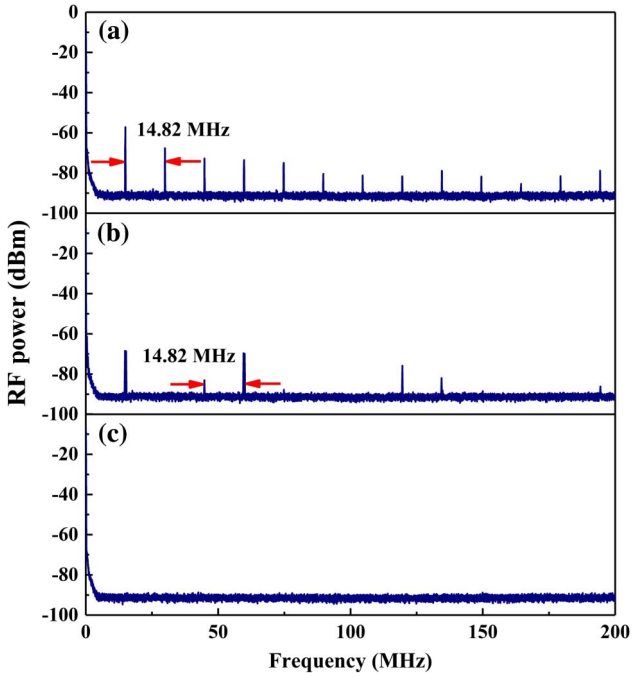

Fig. 6. Laser output beating signal diagram. (a) FBG only; (b) with FBG and FP-FBG; (c) with FBG, FP-FBG, and TCSRs.

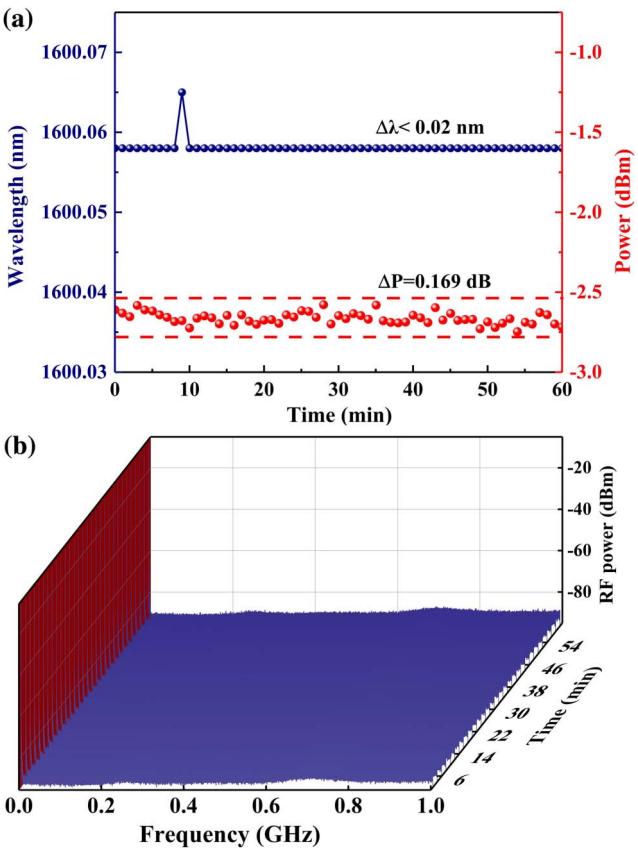

Fig. 7. Output stability of EDFL. (a) Central wavelength and output power; (b) single-longitudinal-mode state.

the SF stability, Fig. 7(b) shows the RF spectrum by repeatedly scanning the ESA at 2-min intervals over a period of 1 h, with an ESA scanning range of 0–1 GHz and an RBW of 100 kHz. Except at zero frequency, no other beating signals and mode-hopping phenomena are found, indicating that the proposed EDFL works in a stable SF state.

The delay self-heterodyne interferometry (DSHI) is a common method for measuring laser linewidth. In experiments, we investigate the laser linewidth by SDSHI, which requires that the delay time is less than the coherence time of the laser. The spectral line of the beating signal generated by the SDSHI is the characteristic coherent envelope[26]. The linewidth is calculated by selecting the two adjacent extreme points of the coherent envelope, the maximum and minimum values, and using the amplitude difference of the extreme points[27]. Compared with the conventional DSHI method, first, it greatly reduces the experimental cost. Second, it avoids transmission loss due to the ultralong fiber, prevents the generation of $1/f$ noise, and effectively suppresses the broadening of the linewidth[28]. The delayed self-heterodyne structure is shown in Fig. 8. The output signal is split into two paths through coupler1. One port is connected to a short-delay fiber. The other port is connected to an acousto-optic modulator (AOM, G-1550-80-L-D-T-AA-A-T-L) to act as a frequency shifter, after which it is connected to the PD via coupler2. The detected signal is displayed on the ESA.

The power spectral density (PSD) function of the beating signal can be expressed as[29,30]

$$S(f)=\frac{P_0^2}{4\pi}\frac{\Delta\nu}{\Delta\nu^2+(f-f_0)^2}\times\left(1-e^{-2\pi\tau_d\Delta\nu}\left(\cos(2\pi\tau_d(f-f_0))+\Delta\nu\frac{\sin(2\pi\tau_d(f-f_0))}{f-f_0}\right)\right)+\frac{\pi P_0^2}{2}e^{-2\pi\tau_d\Delta\nu}\delta(f-f_0),\tag{6}$$

where $\Delta\nu$ is the linewidth of the measured laser, f is the measurement frequency, f_0 is the modulation frequency of the AOM, P_0 is the output laser power, $\tau_d=\frac{nL}{c}$ is the delay time of the fiber and is affected by the fiber length, L is the delay fiber length, and $\delta(f)$ is the pulse function. Selecting a pair of extreme points, S_H and S_L, based on Eq. (6), the relationship between ΔS and $\Delta\nu$ can be expressed as[31]

$$\Delta S=10\log_{10}S_H-10\log_{10}S_L=10\log_{10}\times\frac{\left(\Delta\nu^2+\left(\frac{c}{nL}\right)^2\right)\left(1+e^{-2\pi\left(\frac{nL}{c}\right)\Delta\nu}\right)}{\left(\Delta\nu^2+\left(\frac{3c}{2nL}\right)^2\right)\left(1-e^{-2\pi\left(\frac{nL}{c}\right)\Delta\nu}\right)},\tag{7}$$

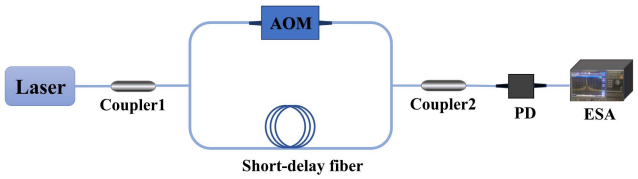

Fig. 8. Schematic of delayed self-heterodyne interferometry for laser linewidth measurement.

where n, L, and c are constant, so the relationship between ΔS and $\Delta\nu$ can be obtained, as shown in Fig. 9(a). As the power density function ΔS decreases, the linewidth $\Delta\nu$ gradually increases. In the process of finding the linewidth, take the pair of neighboring extreme points and calculate the amplitude difference, and after that, substitute into Eq. (7) to get the value of the linewidth.

Due to the influence of system noise, the points far from the center frequency will be submerged by the bottom noise, so that the measured amplitude difference is smaller than the ideal value, and the calculated linewidth is larger than the actual value. Also, since the PD response to the pulse function $\delta(f)$ is unstable at the center frequency and the stability of the AOM frequency shift affects the maximum peak value of the envelope signal, the extreme value points near both sides of the center frequency should be selected. In the experiment, by testing different lengths of fiber, we select a 3-km-long delay fiber. This is because if the fiber is too long, the linewidth will broaden, while if the fiber is too short, the PSD envelope spectrum cannot be clearly observed. The measurement results are shown in Fig. 9(b), where the black curve represents the experimental results and the red curve represents the fitted results. In the fitting process, we simplify the impulse function $\delta(f)$ so it is a smooth envelope at the center frequency, which does not affect the calculation of

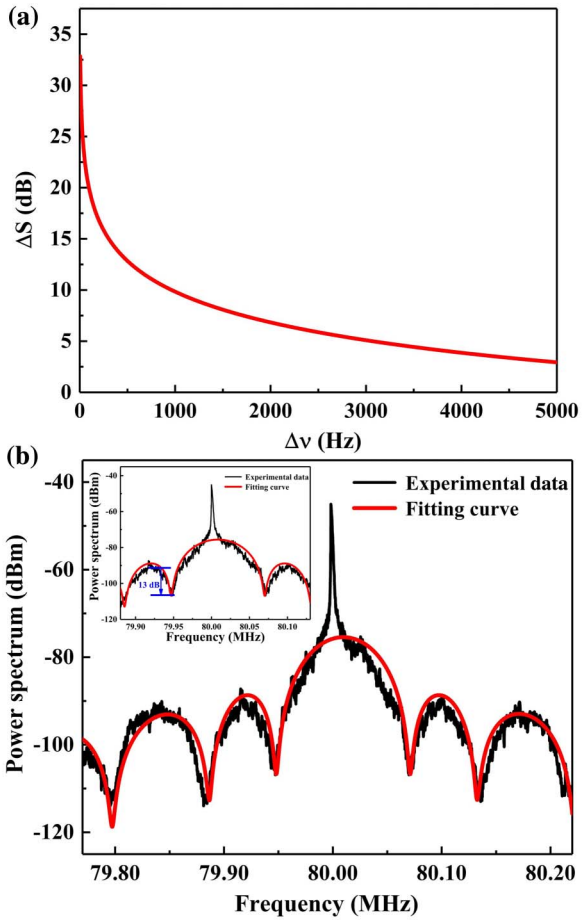

Fig. 9. (a) Relationship between ΔS and $\Delta\nu$; (b) actual detected power spectrum and fitting curve.

amplitude differences. It should be noted that due to the output power limitations and the effect of noise, the actual measured values of the PSD envelope spectrum deviate slightly from the simulated values, and the actual linewidth will be smaller. The inset shows a detailed plot of the signal power spectrum. We select the first minimum and maximum points closest to the center frequency of 80 MHz[27], calculating the amplitude difference ΔS as 13 dB, and obtaining the linewidth of 480 Hz from Fig. 9(a).

4. Conclusion

In summary, we propose an SF EDFL operating at 1.6 μm based on a ring cavity. The beating signals under different cascaded filter devices are observed experimentally using the self-homodyne method, which proves that the laser can work stably in the SF state when FBG and FP-FBG are added into the cavity as well as the TCSRs filter. The TCSRs filter consists of only two couplers for low cost and high filtering capability. The experimental results show that the output wavelength of the laser is stabilized at 1600.06 nm, and the OSNR is higher than 73 dB. During 60 min of continuous monitoring, the central wavelength fluctuation is less than 0.02 nm, and the maximum change in power is 0.169 dB. Additionally, the linewidth of the output laser is measured less than 480 Hz by using the self-built SDSHI device. We realize an all-fiber structured SFFL operating in the 1.6 μm band with high OSNR and narrow linewidth, which has a high potential for applications in coherent lidar and long-distance coherent optical communication and also provides a new idea for the realization of L-band lasers.

Acknowledgements

This work was supported by the Shaanxi Key Science and Technology Innovation Team Project (No. 2023-CX-TD-06).

References

1. Y. Lin, P. Yen, B. Huang, *et al.*, "Applying self-injection and dual-ring based fiber laser for wide tunability and stable single-frequency output," Opt. Laser Technol. **137**, 106804 (2021).
2. R. A. Perez-Herrera, A. Ullan, D. Leandro, *et al.*, "L-band multiwavelength single-longitudinal mode fiber laser for sensing applications," J. Light. Technol. **30**, 1173 (2012).
3. C. Yang, X. Guan, Q. Zhao, *et al.*, "15 W high OSNR kHz-linewidth linearly-polarized all-fiber single-frequency MOPA at 1.6 μm," Opt. Express **26**, 1286 (2018).
4. S. Li, T. Koscica, Y. Zhang, *et al.*, "Optical fiber remote sensing system of methane at 1645 nm using wavelength-modulation technique," Proc. SPIE **5995**, 59950Y (2005).
5. Y. Liu, J. Liu, and W. Chen, "An all-fiber single frequency laser for eye-safe coherent doppler wind lidar," Chin. J. Lasers **36**, 1857 (2009).
6. N. W.-H. Chang, D. J. Hosken, J. Munch, *et al.*, "Stable, single frequency Er: YAG lasers at 1.6 μm," IEEE J. Quantum Electron. **46**, 103 (2010).
7. B. Yao, T. Dai, X. Duan, *et al.*, "Tunable single-longitudinal-mode Er:YAG laser using a twisted-mode technique at 1.6 μm," Laser Phys. Lett. **12**, 025004 (2015).
8. S. Kameyama, M. Imaki, Y. Hirano, *et al.*, "Development of 1.6 μm continuous-wave modulation hard-target differential absorption lidar system for CO_2 sensing," Opt. Lett. **34**, 1513 (2009).
9. X. Guan, Q. Zhao, W. Lin, *et al.*, "High-efficiency and high-power single-frequency fiber laser at 1.6 μm based on cascaded energy-transfer pumping," Photonics Res. **8**, 414 (2020).
10. X. He, X. Fang, C. Liao, *et al.*, "A tunable and switchable single-longitudinal-mode dual-wavelength fiber laser with a simple linear cavity," Opt. Express **17**, 21773 (2009).
11. S. E. Hsieh, C. H. Hsu, C. H. Yeh, *et al.*, "L-band wavelength-selectable erbium laser with stable single-frequency oscillation," Electronics **11**, 2996 (2022).
12. L. Zhang, J. Zhang, Q. Sheng, *et al.*, "Watt-level 1.7-μm single-frequency thulium-doped fiber oscillator," Opt. Express **29**, 27048 (2021).
13. Y. Lai, L. Chen, C. H. Yeh, *et al.*, "Vernier effect based fiber laser with switchable and stable single-mode output behavior," Opt. Quantum Electron. **54**, 378 (2022).
14. Z. Wang, J. Shang, K. Mu, *et al.*, "Stable single-longitudinal-mode dual-ring fiber laser with ultra-narrow linewidth," in *Conference on Lasers and Electro-Optics (CLEO)* (2020), paper STh3P.1.
15. N. F. Razak, H. Ahmad, M. Z. Zulkifli, *et al.*, "Single mode EDF fiber laser using an ultra-narrow bandwidth tunable optical filter," Optik **126**, 179 (2015).
16. H. Ahmad, K. Thambiratnan, M. J. Faruki, *et al.*, "Single longitudinal mode laser generation using coupled microfiber Mach–Zehnder interferometer filter," Laser Phys. **28**, 085102 (2018).
17. C. Yang, X. Guan, W. Lin, *et al.*, "Efficient 1.6 μm linearly-polarized single-frequency phosphate glass fiber laser," Opt. Express **25**, 29078 (2017).
18. L. Huang, C. Yang, T. Tan, *et al.*, "Sub-kHz-linewidth wavelength-tunable single-frequency ring-cavity fiber laser for C-and L-band operation," J. Lightwave Technol. **39**, 4794 (2021).
19. Q. Yang, Y. Wang, C. Yu, *et al.*, "Sub-kHz linewidth 1.6-μm single-frequency fiber laser based on a heavily erbium-doped silica fiber," Opt. Lett. **48**, 2563 (2023).
20. B. Guan, F. Yan, D. Yang, *et al.*, "Sub-kHz narrow-linewidth single-longitudinal-mode thulium-doped fiber laser utilizing triple-coupler ring-based compound-cavity filter," Photonics **10**, 209 (2023).
21. D. Cheng, F. Yan, T. Feng, *et al.*, "Five-wavelength-switchable single-longitudinal-mode thulium-doped fiber laser based on a passive cascaded triple-ring cavity filter," IEEE Photonics J. **14**, 1503608 (2021).
22. S. Pan and J. Yao, "Frequency-switchable microwave generation based on a dual-wavelength single-longitudinal-mode fiber laser incorporating a high-finesse ring filter," Opt. Express **17**, 12167 (2009).
23. T. Feng, M. Jiang, D. Wei, *et al.*, "Four-wavelength-switchable SLM fiber laser with sub-kHz linewidth using superimposed high-birefringence FBG and dual-coupler ring based compound-cavity filter," Opt. Express **27**, 36662 (2019).
24. M. Gao, B. Yin, Y. Lv, *et al.*, "Tunable and switchable dual-wavelength SLM narrow-linewidth fiber laser with a PMFBG-FP filter cascaded by multi-ring cavity," Photonics **9**, 756 (2022).
25. C. Lee, Y. Chen, and S. Liaw, "Single-longitudinal-mode fiber laser with a passive multiple-ring cavity and its application for video transmission," Opt. Lett. **23**, 358 (1998).
26. M. Xue and J. Zhao, "Laser linewidth measurement based on long and short delay fiber combination," Opt. Express **29**, 27118 (2021).
27. Z. Zhao, Z. Bai, D. Jin, *et al.*, "Narrow laser-linewidth measurement using short delay self-heterodyne interferometry," Opt. Express **30**, 30600 (2022).
28. Z. Wang, C. Ke, Y. Zhong, *et al.*, "Ultra-narrow-linewidth measurement utilizing dual-parameter acquisition through a partially coherent light interference," Opt. Express **28**, 8484 (2020).
29. L. Richter, H. Mandelberg, M. Kruger, *et al.*, "Linewidth determination from self-heterodyne measurements with subcoherence delay times," IEEE J. Quantum Electron. **22**, 2070 (1986).
30. Y. Li, Z. Wang, Y. Qin, *et al.*, "Kalman filtering-enhanced short-delay self-heterodyne interferometry for linewidth measurement," Opt. Lett. **48**, 3793 (2023).
31. Z. Zhao, Z. Bai, D. Jin, *et al.*, "The influence of noise floor on the measurement of laser linewidth using short-delay-length self-heterodyne/homodyne techniques," Micromachines **13**, 1311 (2022).